

Short Communication

Investigation of C-Glycosidic Ketone as a Corrosion Inhibitor for Carbon Steel in 3.5% NaCl Saturated Ca(OH)₂ Solution

Jianzhong Liu¹, Dan Zhao^{1,*}, Jingshun Cai¹, Liang Shi¹, Jiaping Liu²

¹ State Key Laboratory of High Performance Civil Engineering Materials, Jiangsu Research Institute of Building Science, Nanjing 211103 (P. R. China)

² Jiangsu Key Laboratory of Construction Materials, College of Materials Science and Engineering, Southeast University, Nanjing 211189 (P. R. China)

*E-mail: zhaodan@cnjsjk.cn

Received: 9 June 2016 / Accepted: 29 July 2016 / Published: 6 September 2016

In this study, a polyhydroxy C-glycosidic ketone (CGK) was synthesized under mild reaction conditions and its activity towards carbon steel in 3.5% NaCl saturated Ca(OH)₂ solution was investigated. Concentration and time dependence of the inhibition effectiveness was acquired by potentiodynamic polarization, electrochemical impedance spectroscopy and cyclic voltammetry. The inhibitor exhibited excellent chemical stability and inhibition efficiency in strong alkaline solution containing high concentration of chloride even after a long exposure time. Results indicated that the CGK acted as a cathodic inhibitor by both physical and chemical adsorption on the steel surface according to the Langmuir adsorption isotherm. The effect of inhibitor addition on the threshold chloride concentration was also assessed, and the CGK could delay corrosion initiation significantly. For further confirming the results obtained from electrochemical measurements, surface morphological observation and analysis were performed using scanning electron microscope, energy dispersive spectroscopy and X-ray diffraction.

Keywords: carbon steel; corrosion inhibitor; simulated concrete pore solution; polyhydroxy derivatives

1. INTRODUCTION

It is well known that concrete is characterized by strong compressive strength, but is comparatively weak in tension and shear. Hence, concrete structures are often strengthened by embedding steel ribs. Meanwhile, corrosion of steel reinforcement induced by chloride is a major deterioration mechanism for concrete structures [1,2]. Over the past decades, in order to eliminate or at least reduce corrosion of steel, several available techniques had been employed, among which the application of corrosion inhibitors was considered more attractive for its easy handling with less

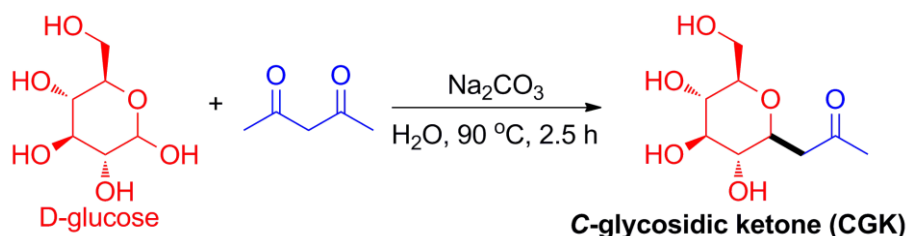
additional cost [3-11]. As typical inorganic inhibitors, nitrites were used as effective anodic inhibitors since the late 1960s [12]. However, the limitations such as carcinogenicity and worse inhibition effect in case of insufficient dosage, should not be ignored [13].

For these reasons, amine-alkanolamine (AMA)-based organic inhibitors were widely studied and commercialized for concrete protection in the last 20 years [14-16]. In recent years, researchers have focused more attention towards developing novel organic inhibitors and some conclusions have been obtained [17-23]. Many literature studies revealed that most of the organic inhibitors decreased the corrosion rates via blocking the active sites on the metal surfaces due to the existence of chemical or physical interactions between iron and heteroatoms such as nitrogen, sulfur, oxygen, phosphorus and multiple bonds or aromatic rings in organic molecules [24-28]. A variety of corrosion inhibitors applied in other corrosive environments or used for other metals have been investigated for steel in concrete or in chloride-contaminated simulated concrete pore (SCP) solution. For example, imidazoline compounds which were widely used for corrosion protection in petroleum industry or acid pickling process also acted as effective inhibitors in protecting carbon steel from corrosion in alkaline chloride solution [29-32]. Additionally, benzotriazole derivatives, well known corrosion inhibitors for copper, could form a complex layer acting as a partial barrier to the access of environment aggressive species on the steel surface [33,34]. Nowadays, polymeric inhibitors are gaining more attention from the research community. The azomethine polyester, usually used against aluminum corrosion could also reduce the corrosion rate of reinforced steel even at very small level [35,36]. Though the above corrosion inhibitors provide sufficient corrosion protection, many of these developments suffer from toxic starting materials and harsh reaction conditions. Besides, these organic inhibitors have potential hazards to the human beings and environment [12,37].

In recent years, from the green and sustainable chemistry point of view, the cheaper, eco-friendly and environmental biocompatible corrosion inhibitors are preferred. Plant extracts are full of organic chemicals, such as alkaloids, flavonoids, terpenes and polyphenolics and they have been studied as environmental friendly inhibitors particularly for acid corrosion [38,39]. Meanwhile, there are a limited number of research works on the use of plant extracts as corrosion inhibitors in concrete or in chloride-contaminated SCP solution, and the known typical examples are plant extracts of bitter leaf [40], mimosa [41] and nopal [42]. However, the active ingredients in the inhibitive action, the mechanism of inhibition and the structure-activity relationship are still superficial [43]. Hence, carrying out the investigations on inhibitive behavior of small biomolecules within plant extracts would contribute to solving these problems, so as to instruct the development of environmental friendly inhibitors scientifically.

Polyhydroxy compounds, such as sorbitol [44], glucose [45] and ascorbic acid [46] derivatives having the ability to form complexes with iron, were studied as effective inhibitors of chloride induced corrosion through the surface complex formation. As one major criterion for evaluating an effective inhibitor is long term stability inside the concrete, but unfortunately, most of the polyhydroxy derivatives are hydrolyzed easily under alkaline aqueous solution. Many polyhydroxy small biomolecules themselves are excellent nutrients which are used to cultivate microorganisms, resulting in degradation very quickly in aqueous solution, and this was the main cause leading to inhibition efficiency loss of natural honey [47,48]. Therefore, the development of alternative polyhydroxy

derivatives with stable chemical structure that can act as effective inhibitors for reinforcing steel in concrete starting from cheap small biomolecules is highly desirable. Moreover, in carbohydrate chemistry, C-glycosides are essentially inert to degradation because the natural anomeric centre has been transformed from a hydrolytically labile O or N acetal link to an ether [49]. Based on the current research status, and in continuation of our research on green organic synthesis [50-54] as well as corrosion inhibitors [55-57], we herein synthesize a C-glycosidic ketone (labeled as CGK, shown in Scheme 1), and we also make fundamental evaluations of this compound. It needs to be pointed out that, CGK was produced via inorganic base mediated domino reaction in water, which presented an efficient synthetic approach to reduce chemical waste and handling costs.



Scheme 1. Synthesis of CGK via base-mediated domino reaction in water.

To the best of our knowledge, this is the first example of CGK applied as a corrosion inhibitor. The objective of this work is to evaluate the influence of the CGK concentration and the time of exposure on the protective properties of steel reinforcement in chloride contaminated SCP solution.

2. EXPERIMENTAL

2.1 Synthesis of CGK

The CGK was prepared and purified by using the procedure described in the literature [58], as shown in Scheme 1. Briefly, to a solution of D-glucose (0.4 mol) in water (200 mL) was added sodium carbonate (0.4 mol) and pentane-2,4-dione (0.48 mol). After stirring at 90 °C for 2.5 h, the precipitate was removed by filtration and the aqueous phase was condensed under reduced pressure to produce pale orange oil. The oil was dissolved in methanol (80 mL) and the resulting precipitate was removed. The solvent was evaporated under reduced pressure to give CGK as orange oil with a quantitative yield. The compound structure was confirmed by Thermo Nicolet/Avatar 370 FT-IR spectrometer.

Fig. 1 shows the FT-IR spectrum of CGK (Before immersion). The peak at 3379 cm^{-1} is ascribed to O–H stretching vibration. The C–H stretching vibration peak appears at 2923 cm^{-1} . The strong peak at 1707 cm^{-1} is ascribed to C=O stretching vibration, which is a main characteristic absorption of CGK. The peaks at 1423 and 1360 cm^{-1} are ascribed to methylene and methyl C–H bending vibrations, respectively. The peak at 1080 cm^{-1} is assigned to the stretching vibration of C–O. These spectrum data is found identical with that described in literature [59], indicating that the target compound has been synthesized correctly.

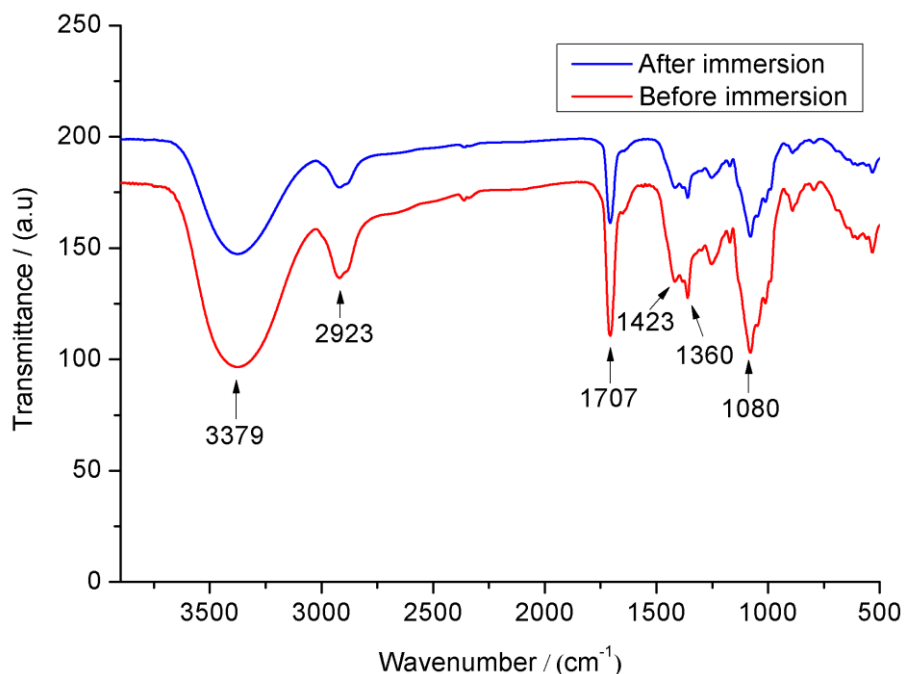


Figure 1. FT-IR spectrum of CGK.

2.2 Materials and sample preparation

The test solution used in all experiments was saturated $\text{Ca}(\text{OH})_2$ solution with 3.5% NaCl prepared from reagent grade chemicals and deionized water.

Working electrodes were cut from the carbon steel bar with a composition (in mass%): C 0.17, Mn 0.46, Si 0.26, Cu 0.019, S 0.017, P 0.0047 and Fe balance. Before measurements, the working electrodes were grinded gradually with grit SiC paper (grade 240, 400, 1000 and 2000), then degreased and rinsed with ethanol.

2.3 Electrochemical measurements

The electrochemical measurements were performed in a conventional three-electrode cell with a volume of 0.37 L, equipped with Ag/AgCl electrode as the reference electrode, platinum mesh sheet as the counter electrode and exposed area of working electrode was 0.36 cm². All the electrochemical experiments were carried out using Parstat 4000 (Princeton Applied Research). Electrochemical impedance spectroscopy (EIS) was performed at the open circuit potential (OCP) in the frequency range of 50 kHz–10 mHz with a 10 mV amplitude signal after the electrodes were immersed in test solutions for 1, 3, 7 and 14d, respectively, using ZSimpWin software to fit the EIS data. Potentiodynamic polarization (PDP) curves were done in the potential range from -200 versus the OCP to the potential at which the current density increased abruptly with a scan rate of 0.5 mV/s. The cyclic voltammetry (CV) curves were recorded in the scan range of -1.2 to -0.1 V versus Ag/AgCl with a scan rate of 20 mV/s. All electrochemical experiments were carried out at room temperature (25 ± 2 °C).

2.4 Threshold chloride concentrations (TCC)

EIS tests utilized a step-by-step increase in chloride concentration to define the threshold chloride concentrations according to the procedure described in the literature [32]. Prior to the tests, the steel electrodes were immersed in SCP solutions without chlorides for 5 days to form a passive layer on steel surface. The steel electrodes were then immersed in the test solutions without and with inhibitor, and the chloride concentration in the solutions was progressively increased (0.05 mol/L NaCl per 24 h). For the EIS tests performed at 24 h after chloride addition, a same three-electrode cell as the above PD, EIS and CV tests was used. EIS was performed at the OCP in the frequency range of 50 kHz–10 mHz with a 10 mV amplitude signal, fitting by ZSimpWin software to obtain the values of resistance. The breakdown of passivity film was detected through the sudden decrease of the resistance.

2.5 Surface morphological observation and analysis

The prepared working electrodes (Φ 18×4 mm) were immersed in 3.5% NaCl saturated Ca(OH)₂ solutions with and without the inhibitor for 3d, respectively. After removal from the test media, the electrodes were rinsed with deionized water and dried with cool air. The topographies of the steel surface were analyzed by scanning electron microscope (SEM, Quanta 250) at an acceleration voltage of 15 kV. Elemental analysis was performed with energy dispersive spectroscopy (EDS, Genesis Apollo X). X-ray diffraction (XRD) analysis was performed by scanning the surface of the test specimens with a scan step of 0.016°, by using Bruker D8 Advance X-Ray Diffractometer. The energy source was Cu K α (1.5418 Å) and the tube settings were 40 kV and 40 mA.

3 RESULTS AND DISCUSSION

3.1 Electrochemical measurements

In order to investigate the interfacial behaviour of steel in the presence of CGK, PDP measurements without (blank) and with various CGK concentrations were performed at the OCP after 3d immersion period, and the curves are shown in Fig. 2. Compared with the blank solution, both anodic and cathodic reactions of carbon steel corrosion in alkaline chloride solution are effectively suppressed, which suggests the inhibitor could reduce the anodic oxidation of iron and also retard the oxygen reduction reaction.

Table 1 collects the fitted electrochemical parameters from PDP curves. E_{corr} , E_{pit} are corrosion potential and pitting potential, respectively. $E_{\text{pit}}-E_{\text{corr}}$ is the width of the passive range and the cathodic (β_c) and anodic (β_a) Tafel slopes are obtained by fitting the polarization data. The degree of surface coverage θ and inhibition efficiency IE are calculated by the following equations:

$$\theta = \frac{i_{corr}^0 - i_{corr}}{i_{corr}^0} \tag{1}$$

$$IE = \frac{i_{corr}^0 - i_{corr}}{i_{corr}^0} \times 100\% \tag{2}$$

where i_{corr}^0 and i_{corr} are the corrosion current densities of the blank and inhibited solutions, respectively. The data reveals that, with increasing the concentration of CGK, i_{corr} decreases significantly, while E_{corr} shifts obviously towards more negative direction. Moreover, the increase of inhibitor concentration would result in a much more positive pitting potential and a wider passive region. Notably, β_c values are significantly altered in presence of inhibitor while β_a values change slightly. Therefore, CGK can be defined as a cathodic inhibitor according to the definite negative shifts of E_{corr} as well as the different variations of Tafel slopes [60].

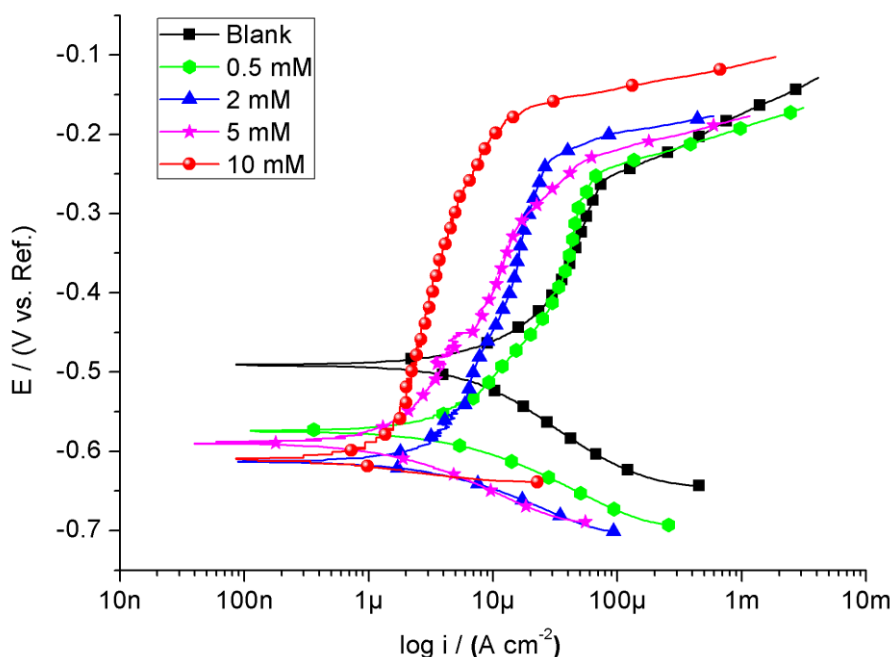


Figure 2. Potentiodynamic polarization curves for carbon steel in 3.5% NaCl sat. Ca(OH)₂ solutions without and with different concentrations of the CGK inhibitor.

Table 1. The electrochemical parameters estimated from PDP data for carbon steel in 3.5% NaCl sat. Ca(OH)₂ solutions with different concentrations of the inhibitor

Conc. (mM)	E_{corr} (mV)	E_{pit} (mV)	$E_{pit}-E_{corr}$ (mV)	I_{corr} ($\mu A cm^{-2}$)	$-\beta_c$ (mV dec ⁻¹)	β_a (mV dec ⁻¹)	θ	IE (%)
Blank	-491	-261	230	13.6	203	189	—	—
0.5	-574	-252	322	4.64	64.1	194	0.659	65.9
2	-613	-226	387	3.31	51.1	385	0.757	75.7
5	-590	-228	362	1.89	76.9	296	0.861	86.1
10	-611	-174	437	0.714	23.4	124	0.948	94.8

EIS studies are further conducted to investigate corrosion inhibition processes in terms of the resistive as well as capacitive behavior at electrode/solution interface. Fig. 3 depicts the EIS responses of the steel electrodes immersed in alkaline chloride solutions in the absence and presence of corrosion inhibitor with various concentrations after 3d immersion period. In comparison with the blank solution, the arc radiuses in Nyquist plots increase significantly in the inhibited solutions, showing the development of a more stable protective film on carbon steel surface with increasing inhibitor concentrations [61]. In Bode plots, impedance modulus at low frequency of the inhibited systems increase, indicating the corrosion is retarded by the CGK. In contrast, the impedance modulus at 10 mHz is about fifty times greater than that in the blank solution when the inhibitor concentration is 10 mM. Moreover, in the presence of inhibitor, the steel electrode exhibits the maximum phase angle value of about 83°, while it is just about 65° in the blank solution, as shown in Fig 3b. Besides, phase angles of inhibited conditions move to lower frequencies indicating the increasing coverage of electrode surface with the adsorption of CGK molecule and/or with the deposition of corrosion products [21].

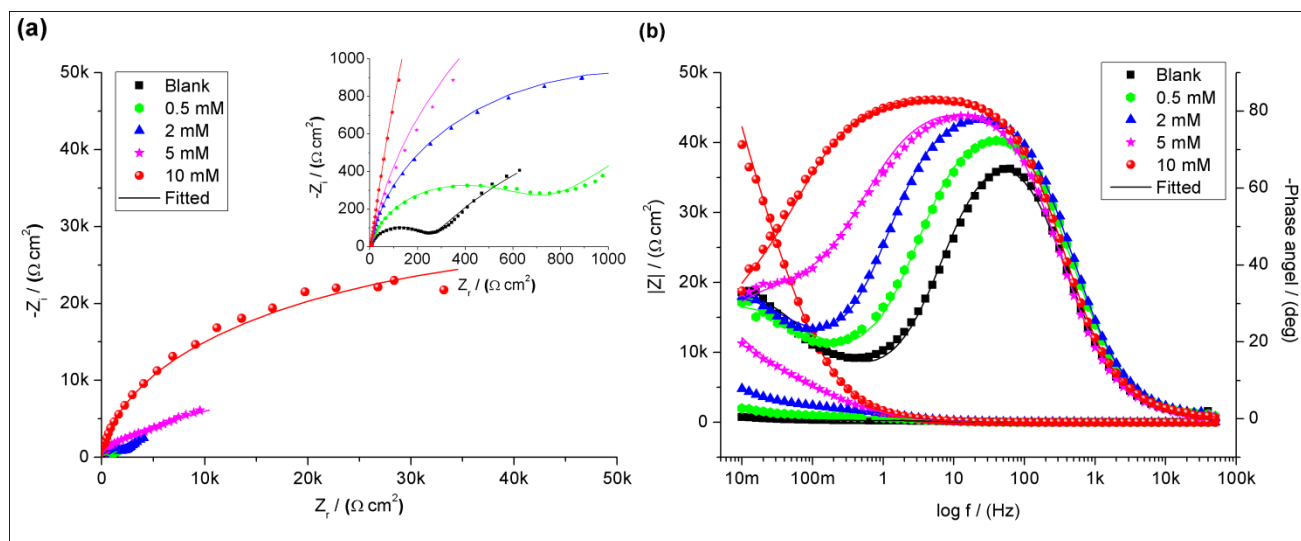


Figure 3. (a) Nyquist and (b) Bode plots for carbon steel in 3.5% NaCl sat. Ca(OH)₂ solutions without and with different concentrations of the CGK inhibitor.

On the basis of the above data and previously reported results, the experimental EIS response is composed of two time constants [62]. The one at high frequencies is attributed to the charge transfer reactions which mainly occur in pores and defects of the steel surface. The other one at low frequencies is related to the behavior of the surface film which consists of the adsorbed inhibitor molecules and/or corrosion products [63]. Therefore, the impedance results could be explained using an equivalent circuit, as shown in Fig 4. In this circuit, R_s represents the electrolyte resistance, R_{ct} represents the charge transfer resistance and R_f is the film resistance. The constant phase elements CPE₁ and CPE₂ are used to replace the double layer capacitance (C_{dl}) and the film capacitance (C_f), respectively. The presence of the constant phase elements are due to the distributed surface heterogeneity, roughness, fractal geometry, electrode porosity, and due to current and potential

distributions related with electrode geometry [64]. It can be seen that the EIS results (Fig. 3) are successfully fitted to above equivalent circuit.

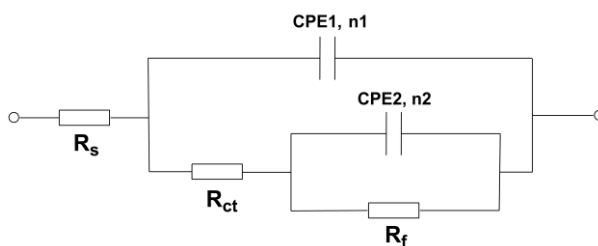


Figure 4. Electrochemical equivalent circuit.

The associated impedance parameters are listed in Table 2, the degree of surface coverage θ and inhibition efficiency IE are calculated by the following equations:

$$\theta = \frac{R_{ct} - R_{ct}^0}{R_{ct}} \quad (3)$$

$$IE = \frac{R_{ct} - R_{ct}^0}{R_{ct}} \times 100\% \quad (4)$$

where R_{ct}^0 and R_{ct} are the charge transfer resistances in uninhibited and inhibited systems, respectively. It is readily apparent that by adding the CGK to the blank solution, the C_{dl} and C_f values tend to decrease. Meanwhile, R_{ct} and R_f values increase significantly with the increase of inhibitor concentration, which is attributed to the formation of a more complete and stable barrier film on the steel surface. The corrosion efficiency obtained from EIS is in good agreement with that from PDP measurements. It is concluded that the inhibitor could increase the pitting potential and strongly hinder the chloride-induced localized corrosion via adsorbing on metal surface and subsequently blocking the active surface sites. Notably, the quality of the fit to the equivalent circuit is judged by the ChiSq value, and low values indicate the results fit the measured data very well [65].

Table 2. The fitted electrochemical parameters from EIS for carbon steel in 3.5% NaCl sat. $\text{Ca}(\text{OH})_2$ solutions with different concentrations of the inhibitor

Conc. (mM)	R_s ($\Omega \text{ cm}^2$)	C_{dl} ($\mu\text{F cm}^{-2}$)	n_1	R_{ct} ($\Omega \text{ cm}^2$)	C_f ($\mu\text{F cm}^{-2}$)	n_2	R_f ($\Omega \text{ cm}^2$)	ChiSq (10^{-3})	θ	IE (%)
Blank	6.16	138.1	0.91	232.8	8766	0.62	2537	0.89	—	—
0.5	6.17	104.2	0.92	680.1	2873	0.57	6569	0.69	0.658	65.8
2	6.01	92.7	0.93	1903	1510	0.64	14170	0.38	0.878	87.8
5	7.17	112.0	0.93	3790	374.5	0.57	27160	0.84	0.939	93.9
10	6.36	103.9	0.94	27220	144.6	0.60	70900	0.41	0.991	99.1

In order to further understand the corrosion mechanism of steel in alkaline chloride solutions, the CV curves were recorded without and with 10 mM CGK at 3d immersion age, as shown in Fig. 5. It is evident that in the blank solution, the anodic peak at -0.62 V can be observed during the anodic

scan process and increases markedly in the 20th cycle. As reported in the literatures [66,67], this peak could be attributed to the formation of $\text{Fe}(\text{OH})_3$ and/or FeOOH by oxidation of $\text{Fe}(\text{II})$ compounds, such as Fe_3O_4 . The potential of the conjugate reduction peak is -0.97 V. In inhibited condition, the corresponding peaks completely disappear within twenty scan cycles and the current density is much lower than that in the blank solution. The amazing results indicate that the inhibitor makes the passive film more stable and inert to chloride in quite high concentration. This helps to explain the high pitting potentials and inhibition efficiencies obtained from PDP and EIS measurements.

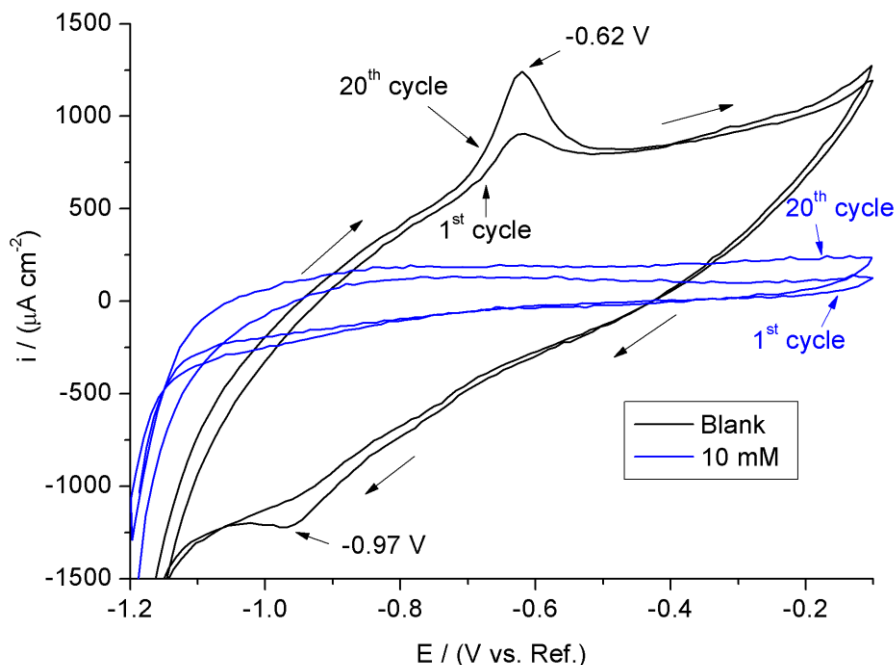


Figure 5. Cyclic voltammety curves for carbon steel in 3.5% NaCl sat. $\text{Ca}(\text{OH})_2$ solutions without and with 10 mM CGK inhibitor.

The stability of adsorbed inhibitor film was also examined with long exposure time test, by PDP and EIS measurements. Fig. 6 presents the PDP curves of the steel in testing solutions without and with 10 mM CGK at different immersion periods, and the fitting values are summarized in Table 3.

The results indicate that the current density decreases between 1 and 3 days of immersion, increases between 3 and 14 days, both for blank and inhibited solutions. The initial decline of current density may be ascribed to the passive film growth at the electrode surface which has been previously reported [68]. The trend is more remarkable for the solutions with inhibitor. It should be noted that, the current density for blank solution decreases at 14d immersion age compared with that at 7d immersion age, while the pitting potential increases significantly (Fig. 6a). This performance is possibly related to the accumulation of the corrosion products at the pit surface with high coverage to prevent the diffusion of reactive corrosive species to steel surface, thus reducing the corrosion rate to a certain extent. Between 7 and 14 days of test, the current density for CGK solution increases, while the inhibition efficiency starts to decrease, but it still remains higher than 80%.

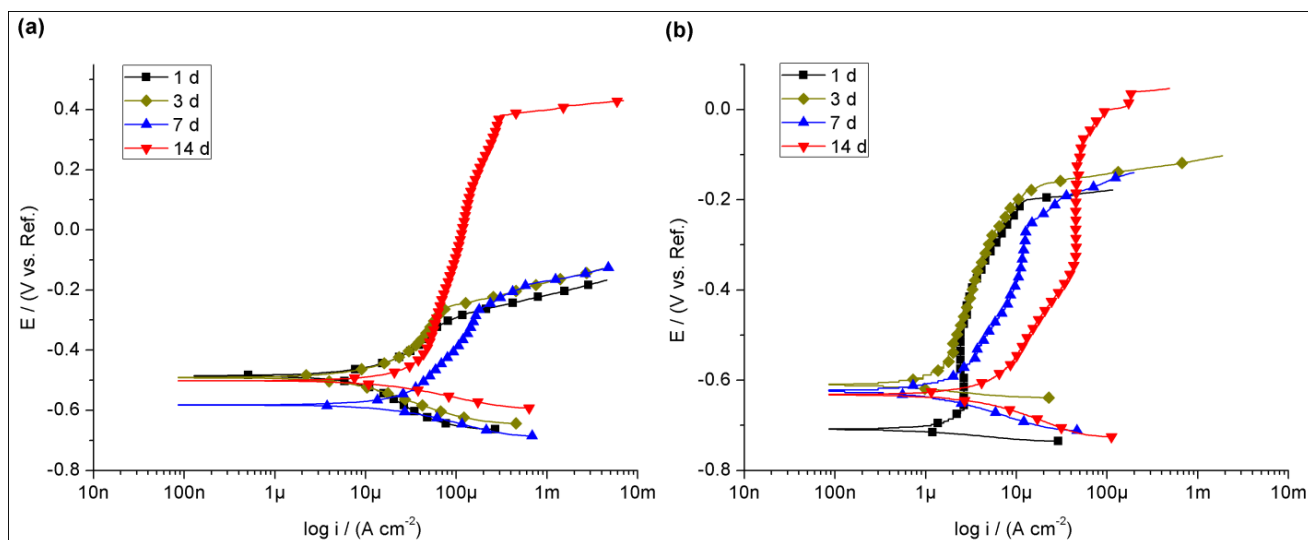


Figure 6. Potentiodynamic polarization curves for carbon steel in 3.5% NaCl sat. Ca(OH)₂ solutions (a) without and (b) with 10 mM CGK inhibitor at different immersion periods.

Table 3. The electrochemical parameters estimated from PDP data for carbon steel in 3.5% NaCl sat. Ca(OH)₂ solutions without and with 10 mM inhibitor at different immersion periods

Time (d)	E _{corr} (mV)	I _{corr} (μA cm ⁻²)	-β _c (mV dec ⁻¹)	β _a (mV dec ⁻¹)	IE (%)
Blank	1	16.5	400	180	—
	3	13.6	203	189	—
	7	35.2	108	460	—
	14	25.3	85.4	286	—
10 mM	1	1.62	26.5	226	90.2
	3	0.714	23.4	124	94.8
	7	1.30	69.6	116	96.3
	14	4.61	78.8	191	81.8

The EIS results were obtained for specimens in solutions without and with 10 mM CGK at different immersion periods, as shown in Fig. 7 and 8, and fitted using the equivalent circuit in Fig. 4. The general trend of the Nyquist diagrams shows a highly depressed capacitive arc from 1 to 14 days of immersion for blank and inhibitor containing solutions, reflecting the evolution of corrosion with time, which is also evidenced by the significant phase angle and impedance modulus drop. For the blank solution, the arc radius in Nyquist plots (Fig. 7a) increases at 14d immersion age compared with that at 7d immersion age, presenting the same corrosion trend with that in PDP measurements (Table 3). As the arc radius in high frequency range at 3d immersion age is larger than that at 1d immersion age for CGK solution (Fig. 8a), the charge transfer resistance has a larger value. Obviously, the resistances for CGK solutions after all immersion times are higher than that for the blank solution.

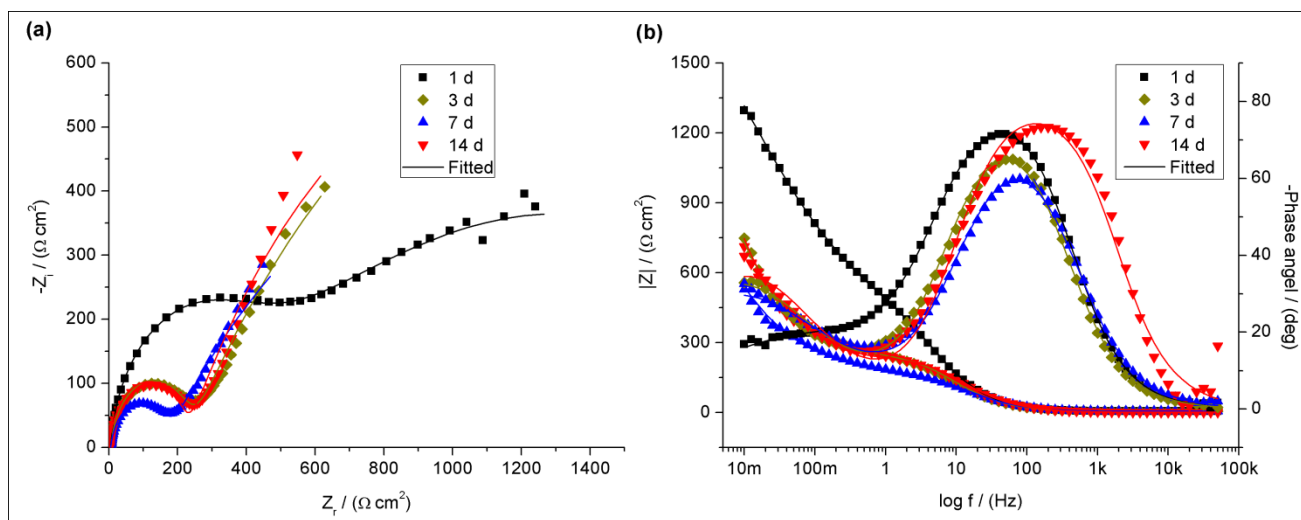


Figure 7. (a) Nyquist and (b) Bode plots for carbon steel in 3.5% NaCl sat. Ca(OH)₂ solutions without inhibitor at different immersion periods.

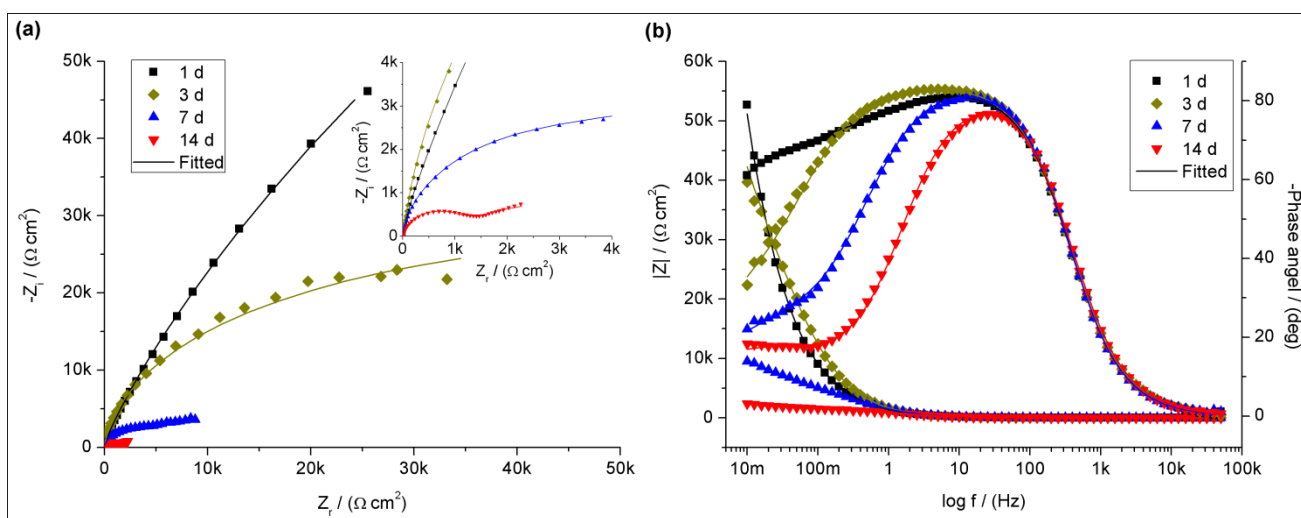


Figure 8. (a) Nyquist and (b) Bode plots for carbon steel in 3.5% NaCl sat. Ca(OH)₂ solutions with 10 mM CGK inhibitor at different immersion periods.

Further, we want to obtain insights into the cause of the decline in inhibition effectiveness after several days of exposure. It should be pointed out that this phenomenon was also observed in the study of carotene as a steel corrosion inhibitor [68]. According to previous investigations [69], ascorbic acid as a chelating agent could assist reductive dissolution of the passive layer at high inhibitor concentrations, resulting in low inhibition efficiency and short pitting initiation time. To help ascertain whether the CGK is also stimulative for iron dissolution, we carried out EIS measurements in CGK solutions at concentrations of 40 and 80 mM, respectively. As shown in Fig. 9, the arc radiuses in the solution with higher concentration are larger, suggesting a better corrosion resistance towards chloride.

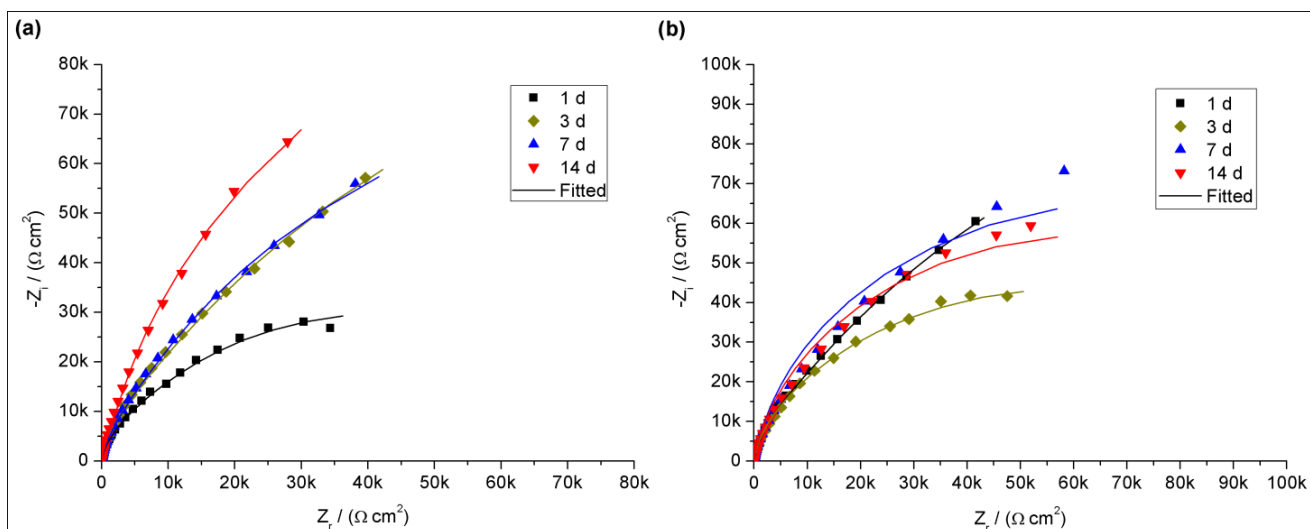


Figure 9. Nyquist plots for carbon steel in 3.5% NaCl sat. Ca(OH)₂ solutions with (a) 40 mM and (b) 80 mM CGK at different immersion periods.

The corresponding EIS data are fitted using the equivalent circuit described in Fig. 4, and the variations of the time dependence of the resistance are shown in Fig. 10. The initial rise of R_{ct} observed in 10 mM solution may be ascribed to the protective film growth at the electrode surface[20]. While the values of R_{ct} in 40 and 80 mM solutions keep stable, due in part to quick formation of absorption film with highly stability. The R_{ct} values in the presence CGK are much higher than that of blank solution within the immersion periods, revealing that the inhibitor has a good inhibition effect for reinforcing steel in chloride contaminated SCP solution. Accordingly, the possibility of the passive layer dissolution via the formation of soluble iron chelate, could be excluded. Besides, these results also showed that CGK was more controllable in inhibitive behavior than ascorbic acid.

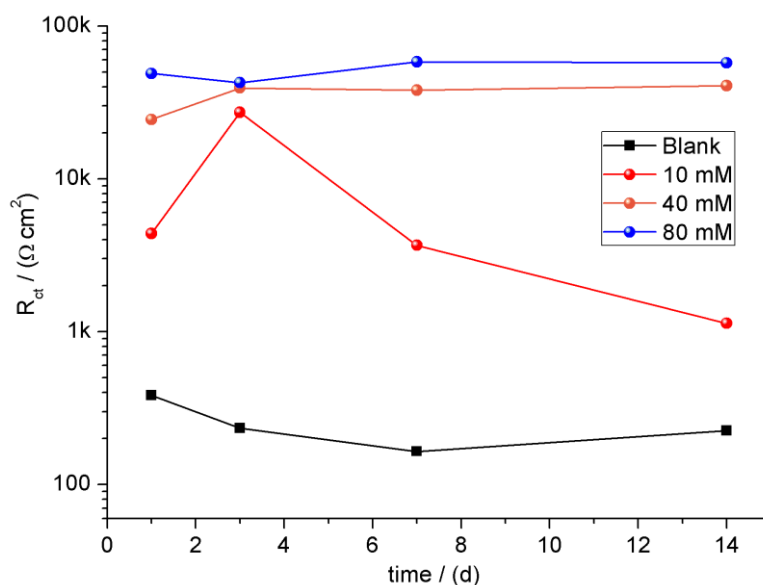


Figure 10. The variations of resistance for carbon steel in 3.5% NaCl sat. Ca(OH)₂ solutions without and with CGK inhibitor at different immersion periods.

The chemical stability of inhibitor compound is a crucial matter for long-term practical applications, therefore the weakening inhibition effectiveness is probably because of the destruction of inhibitor compound in strong alkaline solution. To verify this hypothesis, a control experiment has been performed. The CGK (10 mM) was dissolved in saturated $\text{Ca}(\text{OH})_2$ solution at room temperature ($25 \pm 2 \text{ }^\circ\text{C}$) for 14 days. Then the solution was condensed under reduced pressure, and the obtained oil was dissolved in methanol, removing the resulting precipitate. The solvent was evaporated to afford orange oil. The FT-IR spectrum was recorded and compared with that of CGK, as shown in Fig. 1 (After immersion). We can see that, no obvious difference is detected, indicating the highly stability of CGK under alkaline condition. Although, the cause of the decline in inhibition effectiveness is not clear according to the above experiments, it could be explained via the following threshold chloride concentration analysis. We believe that the corrosion initiation could be delayed by increasing the inhibitor content and in fact the mass fraction is 0.22% for 10 mM CGK solution, not high in practical application.

3.2 Threshold chloride concentration analysis

EIS tests was previously employed to determine the threshold chloride concentration (TCC) value, which is defined as the content of chloride that is necessary to destroy the passive layer on the steel surface and initiate the corrosion process [1]. Thus, TCC value represents the difficulty of the passive film breakdown as well as the ability of corrosion inhibitors to delay the corrosion initiation. The Nyquist plots of steels in blank solution and 10 mM CGK solution, were shown in Fig. 11. Obviously, the Nyquist plots obtained for the steel electrodes in blank solution displays a large arc radius at the first day (the chloride concentration is 0.05 M). However, once the chloride concentration is up to 0.10 M, the capacitive arcs shrink rapidly, which was proved once in the literature[70]. For steel in CGK solution, the capacitive arcs show some fluctuation but no notable change during the first seven days, and the arc radius is far larger than that for the blank solution at the same immersion time. But the capacitive arcs also shrink along with the immersion time prolonged, indicating the destruction of the passive film on the steel surface and corrosion initiation in the presence of aggressive chloride.

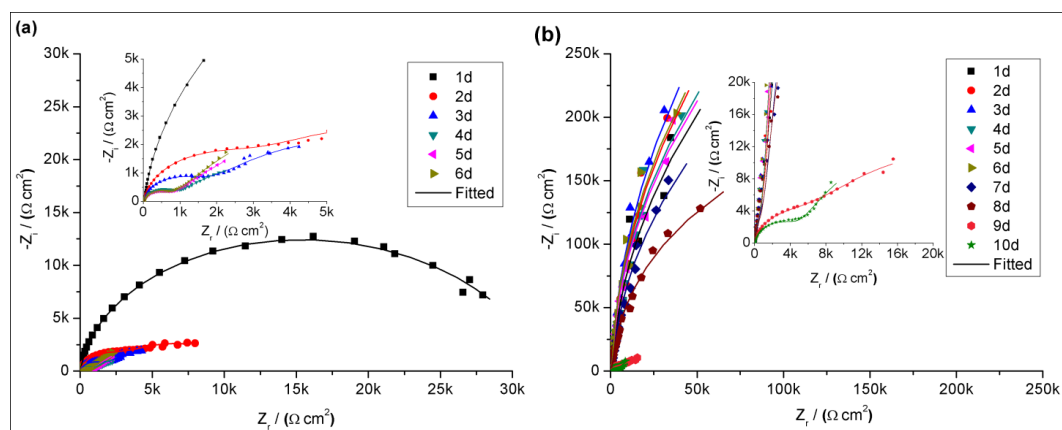


Figure 11. The evolutions of Nyquist plots for carbon steel in sat. $\text{Ca}(\text{OH})_2$ solutions containing chloride (a) without inhibitor; (b) with 10 mM CGK.

The values of R_{ct} for the blank and inhibited solution were fitted using the above equivalent circuit, and were shown in Fig. 12. It can be seen that, in the blank solution, the R_{ct} value decreases quite quickly once the chloride concentration reaches to 0.10 M, but then decreases very slowly. In contrast, in the presence of CGK, the R_{ct} value exhibits a very different trend. The R_{ct} stays at a very large value until the chloride concentration is above 0.35 M. The TCC experiments suggested that the CGK absorbed on the steel surface could protect the steel from corrosion initiation within a wide range of chloride concentration. Considering that the concentration of chloride used in long exposure time test was 3.5% (about 0.6 M), the observed decline in inhibition effectiveness within 7 days was reasonable.

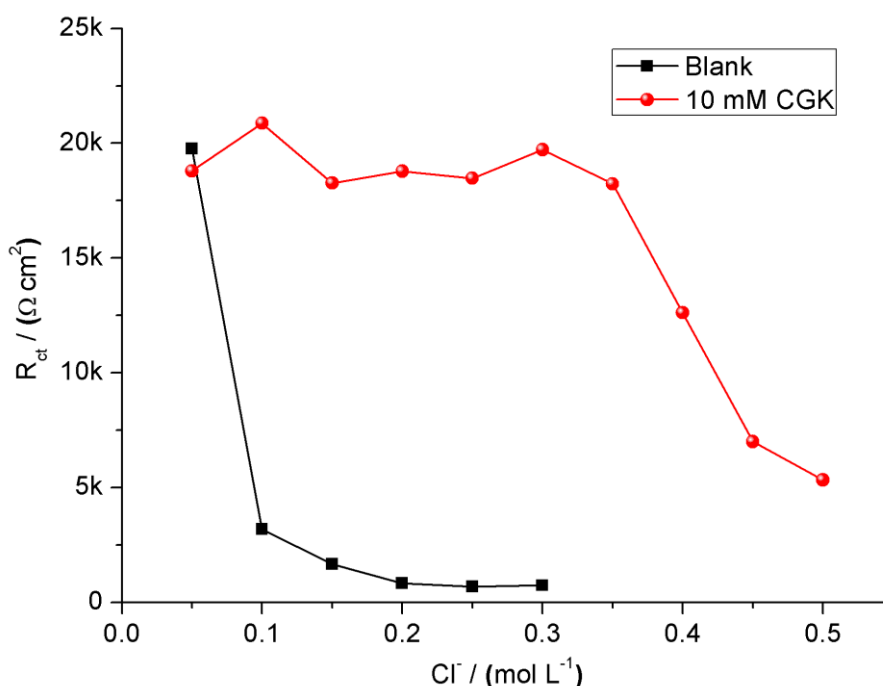


Figure 12. The variations of R_{ct} for carbon steel in sat. $\text{Ca}(\text{OH})_2$ solutions containing chloride without and with inhibitor.

3.3 Adsorption isotherm

With the degree of surface coverage θ in different concentrations obtained by PDP and EIS measurements, as shown in Table 1 and 2, respectively, further investigations were focused on the adsorption behaviour of CGK on the steel surface. In the present investigation, we found that the adsorption of the CGK obeyed the Langmuir adsorption isotherm. According to Langmuir isotherm, the degree of surface coverage θ is related to inhibitor concentration C as [71]:

$$\frac{C}{\theta} = \frac{1}{K_{ads}} + C \quad (5)$$

where K_{ads} is the adsorption equilibrium constant.

The linear-relationship between C/θ and C is plotted in Fig. 13 and the two fitted lines are in good agreement. The subscripts P and E represent the measurements of the PDP and EIS, respectively.

The line slope and correlation coefficient R^2 are close to 1, confirming the good agreement between experimental results and Langmuir adsorption isotherms.

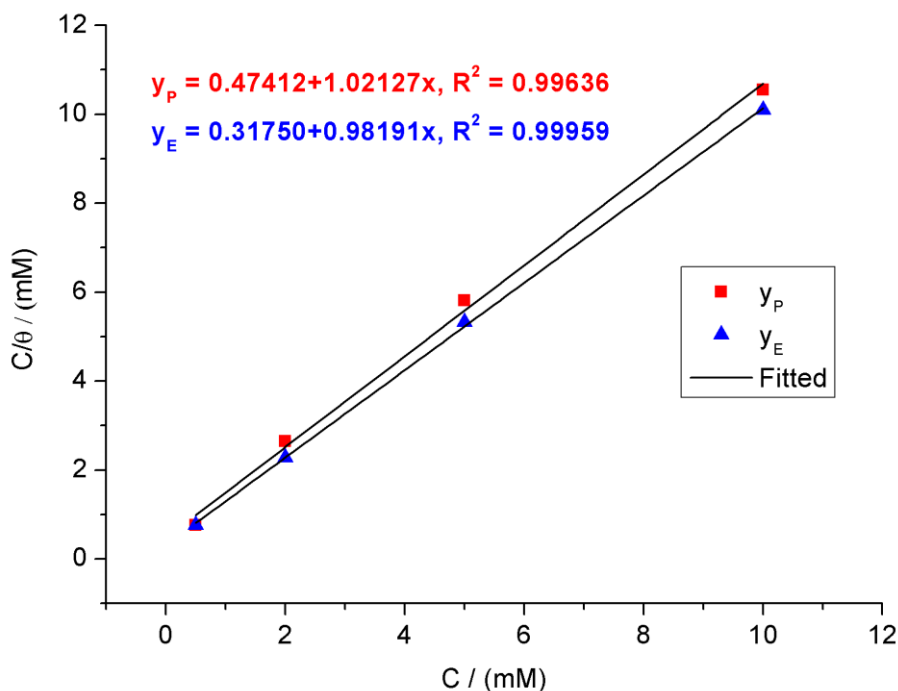


Figure 13. Langmuir adsorption isotherm of the CGK inhibitor on carbon steel surface.

The related standard free energy of adsorption ΔG_{ads}^0 can be estimated by the following equation:

$$K_{ads} = \frac{1}{55.5} \exp\left(-\frac{\Delta G_{ads}^0}{RT}\right) \quad (6)$$

where the numeral of 55.5 is the molar concentration of water in solution, R is the universal gas constant, and T is the absolute temperature (298 K in this work). Generally, the value of ΔG_{ads}^0 up to -20 kJ mol^{-1} indicated a physical adsorption, while negative than -40 kJ mol^{-1} involved sharing or transferring of electrons between the inhibitor molecule with the metal surface to form a coordinate type bond (chemical adsorption) [72]. The calculated ΔG_{ads}^0 values were -28.9 and $-29.9 \text{ kJ mol}^{-1}$ calculated from PDP and EIS measurements, respectively. This result indicated that the inhibitor’s adsorption on steel surface might involve both physical and chemical adsorption processes.

3.4 Surface morphological observation and analysis

To examine the corrosion state of steel reinforcement in alkaline chloride solution without and with inhibitor, the micrographs of steel after 3d immersion were observed by SEM, and compared with that of steel with no immersion (Fig. 14).

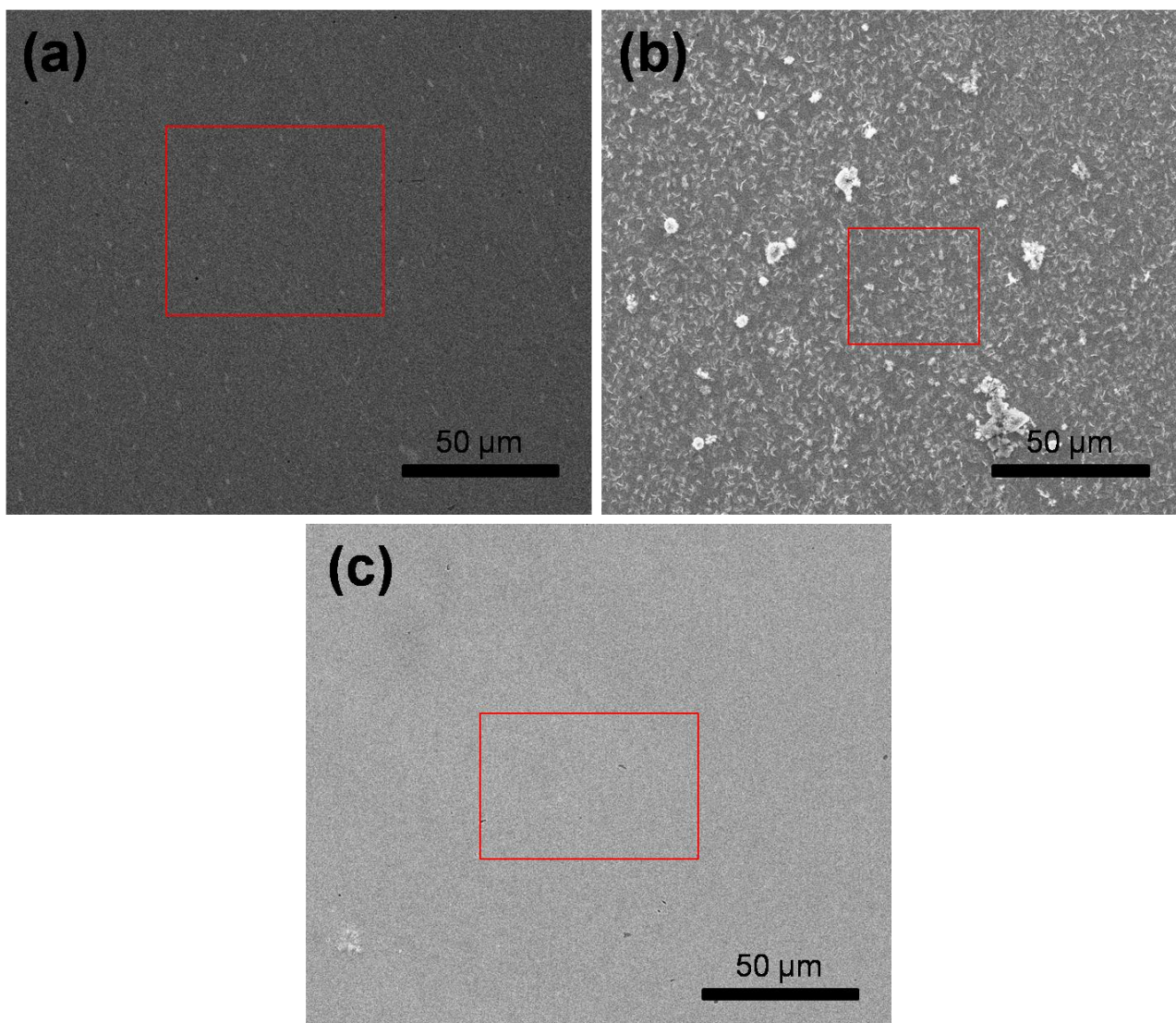


Figure 14. Morphological observation of the steel surface via SEM analysis (a) before immersion and immersed in 3.5% NaCl sat. $\text{Ca}(\text{OH})_2$ solutions (b) without inhibitor; (c) with 10 mM CGK.

It can be seen that, the sample immersed in the blank solution suffers from a severe corrosion damage, while the surface of the steel in CGK solution is smooth and clean, similar to the one with no immersion.

Visual inspection in Fig. 15 also shows significant differences and there is a white deposition layer on the steel surface for the sample in blank solution. The above observations are consistent with the results from the electrochemical measurements. Further, the detailed surface analysis via EDS shows an estimation of the composition of major chemical elements on the steel surface. The scanning area is highlighted in the SEM image with a red-lined box, as shown in Fig. 14. For simplicity, the total element content is normalized to 100% by weight. Fig. 15 shows the characteristics peaks of the selected elements, including Fe, C, O and Ca, and the exact content is shown in Fig. 16. Generally, the iron content is considerably suppressed relative to the samples immersed in the blank solution, in comparison with that before immersion. Meanwhile, for the sample immersed in 10 mM CGK solution, the iron content is nearly unchanged. Additionally, there is no obvious change in carbon

content for all the immersed samples, in sharp contrast, both the oxygen and calcium contents increase significantly for the sample in the blank solution. The results indicate that the white heap on the steel surface in the SEM image (Fig. 14) may not be CaCO_3 , otherwise the carbon content would increase proportionally. Besides, there is no doubt that the increase in oxygen content is due to accumulation of corrosion product on the steel surface, such as iron oxides type compound [32].

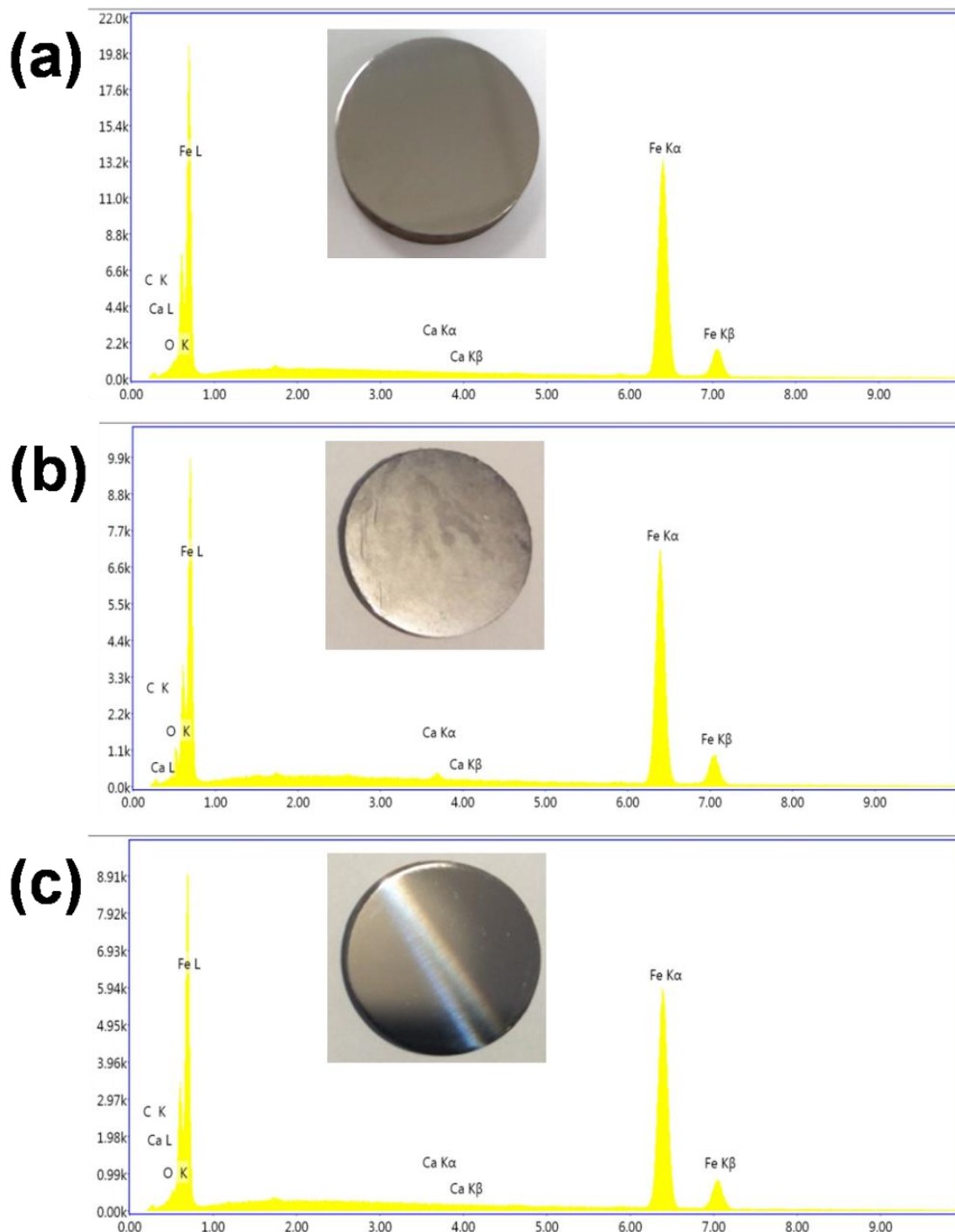


Figure 15. EDS analysis (a) before immersion and immersed in 3.5% NaCl sat. $\text{Ca}(\text{OH})_2$ solutions (b) without inhibitor; (c) with 10 mM CGK, where the photographs of steel electrodes are also present.

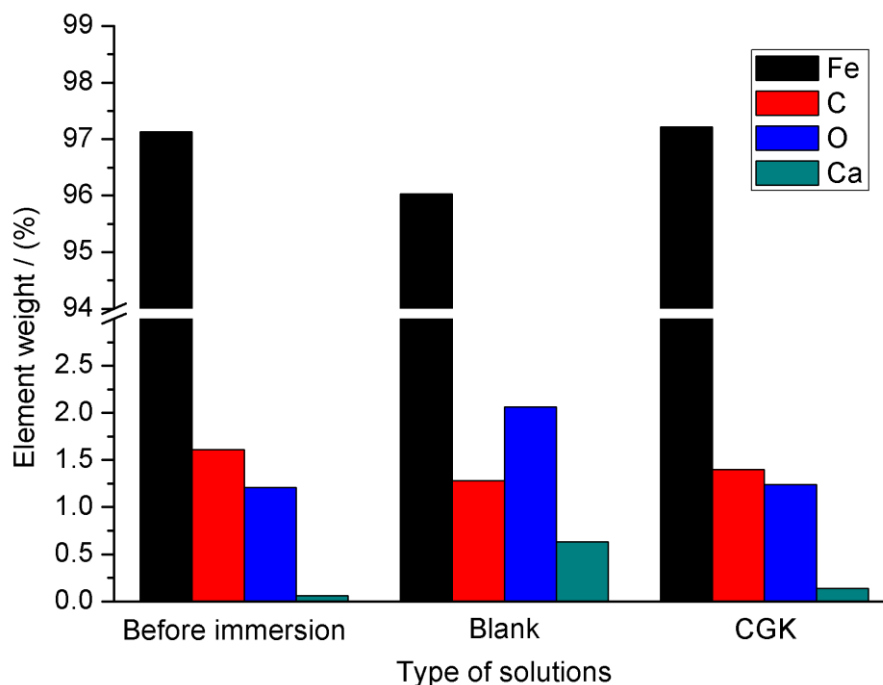


Figure 16. Element content of the carbon steel surface.

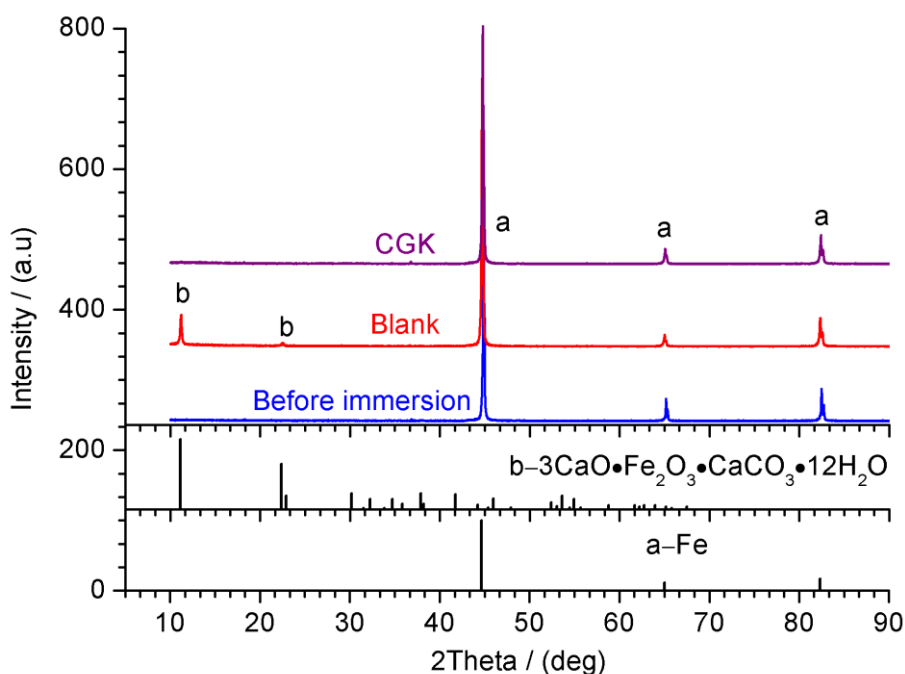


Figure 17. XRD patterns for the carbon steel before immersion and immersed in 3.5% NaCl sat. Ca(OH)₂ solutions without and with inhibitor.

To further investigate the corrosion product, XRD analysis was performed by scanning the surface of the test specimens after 3d immersion, as shown in Fig. 17. The main phases were identified and their characteristic reflections are shown on the bottom of Fig. 17. In the presence of 10 mM CGK, only pure iron characteristic reflections are detected, corresponding to the peaks of 44.8°, 65.1° and

82.4°, which is similar to the specimen before immersion. For specimens in the blank solution, an unexpected crystalline phase is observed, corresponding to the peaks of 11.2° and 22.5°. Based on fundamental of chemical precipitation, we supposed the diffraction patterns most likely presented calcium iron oxide carbonate hydrate ($3\text{CaO}\cdot\text{Fe}_2\text{O}_3\cdot\text{CaCO}_3\cdot 12\text{H}_2\text{O}$) which matched with the phase observed here better than other potential compounds.

These results supported the hypothesis that corrosion product accumulated on the steel surface was an iron oxides type complex. It was possible that iron dissolved readily and formed less stable compounds with oxides and hydroxides, subsequently reacted with chloride ions to form a soluble complex, thereby creating favourable conditions for corrosion product precipitation in the presence of $\text{Ca}(\text{OH})_2$. It should be noted the phase of common hematite (Fe_2O_3), lepidocrocite (FeOOH) or calcite (CaCO_3) were not observed for all test specimens [32]. The XRD analysis further supported the results derived from the above morphological observations and EDS analysis of the steel surface.

4. CONCLUSIONS

In summary, polyhydroxy C-glycosidic ketone (CGK) corrosion inhibitor has been synthesized under mild reaction conditions in water. This compound was prepared from a cheap small biomolecule D-glucose which is eco-friendly. Moreover, the highly stability of CGK under alkaline condition was confirmed by FT-IR spectroscopy. We also made fundamental evaluations of this compound in various concentrations using electrochemical techniques as well as surface analysis. The CGK exhibited a superior inhibition performance in 3.5% NaCl SCP solution, and it could significantly increase the corrosion resistance of the steel reinforcement during long time exposure. The maximum inhibition efficiency of 99.1% was observed at 10 mM concentration. Cyclic voltammetry experiments confirmed that the CGK could effectively suppress the localised corrosion induced by chloride. Besides, the inhibitive behavior in high concentrations (40 and 80 mM) showed that CGK was more controllable than the previously studied ascorbic acid in literature. Meanwhile, the 10 mM CGK corrosion inhibitor increased the threshold chloride concentration for corrosion initiation significantly, comparing with the blank solution. The adsorption of CGK corresponded well with Langmuir isotherm. The standard adsorption free energy was -28.9 and -29.9 kJ mol^{-1} calculated from PDP and EIS measurements, respectively, which indicated both physical and chemical adsorption on the steel surface. The visual inspection and SEM analysis verified that the CGK could strongly inhibit corrosion product forming on the steel surface. EDS and XRD analysis revealed that the corrosion product might be an iron oxides type complex.

The present study provides a novel and efficient organic inhibitor, and we wish the work could help to instruct the development of environmental friendly inhibitors scientifically. Ongoing research involves further application of this inhibitor in reinforced concrete and the evaluation of other synthetic polyhydroxy derivatives is currently underway in our laboratory.

ACKNOWLEDGEMENTS

This work was supported by the National Basic Research Program of China (No. 2015CB655105), National Natural Science Foundation of China (No. 51308261, 51508242) and Natural Science Foundation of Jiangsu Province of China (BK20151012, BK20160104, BK20161101).

References

1. K. Y. Ann and H.-W. Song, *Corros. Sci.*, 49 (2007) 4113.
2. S. Hara, M. Miura, Y. Uchiumi, T. Fujiwara and M. Yamamoto, *Corros. Sci.*, 47 (2005) 2419.
3. V. Kumar, *Corros. Rev.*, 16 (1998) 317.
4. E. A. H. Al Zubaidy and A. Al Tamimi, *Int. J. Electrochem. Sci.*, 7 (2012) 6472.
5. P. Faustino, A. Bras and T. Ripper, *Mater. Struct.*, 48 (2015) 1303.
6. P. Faustino, A. Brás and T. Ripper, *Construct. Build. Mater.*, 53 (2014) 360.
7. G. K. Glass, A. M. Hassanein and N. R. Buenfeld, *Corros. Sci.*, 43 (2001) 1111.
8. J. M. Miranda, J. A. González, A. Cobo and E. Otero, *Corros. Sci.*, 48 (2006) 2172.
9. S. Erdogdu, T. W. Bremner and I. L. Kondratova, *Cem. Concr. Res.*, 31 (2001) 861.
10. N. Gowripalan and H. M. Mohamed, *Cem. Concr. Res.*, 28 (1998) 1119.
11. Y. Liu and X. Shi, *Corros. Rev.*, 27 (2009) 53.
12. P. B. Raja, S. Ghoreishiamiri and M. Ismail, *Surf. Rev. Lett.*, 22 (2015) 1550040.
13. X. Zhou, H. Y. Yang and F. H. Wang, *Electrochim. Acta*, 56 (2011) 4268.
14. L. B. Mechmeche, L. Dhouibi, M. Ben Oueddou, E. Triki and F. Zucchi, *Cem. Concr. Compos.*, 30 (2008) 167.
15. H. B. Zheng, W. H. Li, F. B. Ma and Q. L. Kong, *Construct. Build. Mater.*, 37 (2012) 36.
16. F. Wombacher, U. Maeder and B. Marazzani, *Cem. Concr. Compos.*, 26 (2004) 209.
17. N. Ettayeb, L. Dhouibi, H. Takenouti and E. Triki, *Cem. Concr. Compos.*, 55 (2015) 241.
18. M. Criado, C. Monticelli, S. Fajardo, D. Gelli, V. Grassi and J. M. Bastidas, *Construct. Build. Mater.*, 35 (2012) 30.
19. O. Vololonirina, A. Sellier and G. Arliguie, *Construct. Build. Mater.*, 37 (2012) 541.
20. J.-H. Li, B. Zhao, J. Hu, H. Zhang, S.-G. Dong, R.-G. Du and C.-J. Lin, *Int. J. Electrochem. Sci.*, 10 (2015) 956.
21. X. Zhou, H. Yang and F. Wang, *Electrochim. Acta*, 56 (2011) 4268.
22. E.-S. M. Sherif, *Int. J. Electrochem. Sci.*, 7 (2012) 4834.
23. A. S. Fouda, G. Y. Elewady, K. Shalabi and H. K. A. El-Aziz, *RSC Adv.*, 5 (2015) 36957.
24. M. Ormellese, L. Lazzari, S. Goidanich, G. Fumagalli and A. Brenna, *Corros. Sci.*, 51 (2009) 2959.
25. S. M. Abd El Haleem, S. Abd El Wanees and A. Bahgat, *Corros. Sci.*, 87 (2014) 321.
26. A. B. da Silva, E. D'Elia and J. Gomes, *Corros. Sci.*, 52 (2010) 788.
27. V. R. Saliyan and A. V. Adhikari, *Corros. Sci.*, 50 (2008) 55.
28. Z. Zhang, S. Chen, Y. Li, S. Li and L. Wang, *Corros. Sci.*, 51 (2009) 291.
29. P. C. Okafor and Y. Zheng, *Corros. Sci.*, 51 (2009) 850.
30. S.-H. Yoo, Y.-W. Kim, K. Chung, S.-Y. Baik and J.-S. Kim, *Corros. Sci.*, 59 (2012) 42.
31. T. Gu, P. Su, X. Liu, J. Zou, X. Zhang and Y. Hu, *J. Petrol. Sci. Eng.*, 102 (2013) 41.
32. F.-l. Fei, J. Hu, J.-x. Wei, Q.-j. Yu and Z.-s. Chen, *Construct. Build. Mater.*, 70 (2014) 43.
33. S. Liu, J. M. Duan, R. Y. Jiang, Z. P. Feng and R. Xiao, *Mater. Corros.*, 62 (2011) 47.
34. M. M. Mennucci, E. P. Banczek, P. R. P. Rodrigues and I. Costa, *Cem. Concr. Compos.*, 31 (2009) 418.
35. B. J. Vasanthi, L. Ravikumar and A. Selvaraj, *Mater. Corros.*, 59 (2008) 14.
36. B. Bhuvaneshwari, A. Selvaraj, N. R. Iyer and L. Ravikumar, *Mater. Corros.*, 66 (2015) 387.
37. P. B. Raja and M. G. Sethuraman, *Mater. Lett.*, 62 (2008) 113.
38. N. M'hiri, D. Veys-Renaux, E. Rocca, I. Ioannou, N. M. Boudhrioua and M. Ghoul, *Corros. Sci.*, 102 (2016) 55.
39. A. Ostovari, S. M. Hoseinie, M. Peikari, S. R. Shadizadeh and S. J. Hashemi, *Corros. Sci.*, 51 (2009) 1935.
40. C. A. Loto, O. O. Joseph, R. T. Loto and A. P. I. Popoola, *Int. J. Electrochem. Sci.*, 8 (2013) 11087.

41. S. Martinez, L. Valek and I. S. Oslakovic, *J. Electrochem. Soc.*, 154 (2007) C671.
42. A. A. Torres-Acosta, *J. Appl. Electrochem.*, 37 (2007) 835.
43. P. Mourya, S. Banerjee and M. M. Singh, *Corros. Sci.*, 85 (2014) 352.
44. X. Zhou, H.-Y. Yang and F.-H. Wang, *Acta Phys.-Chim. Sin.*, 27 (2011) 647.
45. X. Zhou, H. Yang and F. Wang, *Corros. Sci.*, 54 (2012) 193.
46. L. Feng, H. Yang and F. Wang, *Acta Chim. Sinica*, 69 (2011) 2359.
47. A. Y. El-Etre and M. Abdallah, *Corros. Sci.*, 42 (2000) 731.
48. A. Y. El-Etre, *Corros. Sci.*, 40 (1998) 1845.
49. F. Rodrigues, Y. Canac and A. Lubineau, *Chem. Commun.*, (2000) 2049.
50. D. Zhao, Y.-R. Zhou, Q. Shen and J.-X. Li, *RSC Adv.*, 4 (2014) 6486.
51. D. Zhao, Y. Wang, M.-X. Zhu, Q. Shen, L. Zhang, Y. Du and J.-X. Li, *RSC Adv.*, 3 (2013) 10272.
52. D. Zhao, T. Wang and J.-X. Li, *Chem. Commun.*, 50 (2014) 6471.
53. D. Zhao, T. Wang, Q. Shen and J.-X. Li, *Chem. Commun.*, 50 (2014) 4302.
54. D. Zhao, Q. Shen and J.-X. Li, *Adv. Synth. Catal.*, 357 (2015) 339.
55. J. Z. Liu, D. Zhao, J. S. Cai, L. Shi and J. P. Liu, *Int. J. Electrochem. Sci.*, 11 (2016) 1135.
56. J. Cai, C. Chen and J. Liu, *Corros. Eng. Sci. Technol.*, 49 (2014) 66.
57. J. P. Liu, C. C. Chen, J. S. Cai, J. Z. Liu and G. Cui, *Mater. Corros.*, 64 (2013) 1075.
58. J. Wang, Q. Li, Z. Ge and R. Li, *Tetrahedron*, 68 (2012) 1315.
59. L. Yan, F.-W. Liu, J.-L. Yang and H.-M. Liu, *J. Carbohydr. Chem.*, 26 (2007) 339.
60. Z. Tao, S. Zhang, W. Li and B. Hou, *Corros. Sci.*, 51 (2009) 2588.
61. H. E. Jamil, M. F. Montemor, R. Boulif, A. Shriri and M. G. S. Ferreira, *Electrochim. Acta*, 48 (2003) 3509.
62. M. A. Migahed, A. A. Attia and R. E. Habib, *RSC Adv.*, 5 (2015) 57254.
63. L. Feng, H. Yang and F. Wang, *Electrochim. Acta*, 58 (2011) 427.
64. B. Dong, Y. Wang, W. Ding, S. Li, N. Han, F. Xing and Y. Lu, *Construct. Build. Mater.*, 56 (2014) 1.
65. C. Sun, S. Liu, J. Niu and W. Xu, *Int. J. Electrochem. Sci.*, 10 (2015) 5309.
66. L. Yohai, M. Vazquez and M. B. Valcarce, *Electrochim. Acta*, 102 (2013) 88.
67. M. Cabrini, S. Lorenzi and T. Pastore, *Electrochim. Acta*, 124 (2014) 156.
68. M. A. Ameer, *Mater. Chem. Phys.*, 122 (2010) 321.
69. L. Valek, S. Martinez, D. Mikulic and I. Brnardic, *Corros. Sci.*, 50 (2008) 2705.
70. J. Xu, L. Jiang and F. Xing, *Mater. Corros.*, 61 (2010) 802.
71. M. S. Morad, *J. Appl. Electrochem.*, 38 (2008) 1509.
72. M. Bouklah, B. Hammouti, M. Lagrenee and F. Bentiss, *Corros. Sci.*, 48 (2006) 2831.